

Research Article

Scaling vesicle distributions and volcanic eruptions

Hélène Gaonac¹ , Shaun Lovejoy² and Daniel Schertzer³

(1) GEOTOP, UQÀM, Succ. Centre-Ville, C.P. 8888, Montréal, Qc., H3C 3P8, Canada

(2) Department of Physics, McGill University, Montréal, Qc., H3A 2T8, Canada

(3) Ecole Nationale des Ponts et Chaussées, 6–8, avenue Blaise Pascal, Cité Descartes, 77455 Marne la Vallée Cedex, France

 **Hélène Gaonac¹**

Email: gaonach.helene@uqam.ca

Phone: +1-514-987-3000 ext 1968

Fax: +1-514-987-3635

Received: 3 June 2003 **Accepted:** 10 March 2004 **Published online:** 19 August 2004

Abstract Models of coalescence-decompressive expansion of the later stages of bubble growth predict that for diverse types of volcanic products the vesicle number densities ($n(V)$) are of the scaling form $n(V) \propto V^{-B_3-1}$ where V is the volume of the vesicles and B_3 the 3-dimensional scaling (power law)

exponent. We analyze cross sections of 9 pumice samples showing that over the range of bubble sizes from $\approx 10 \mu\text{m}$ to 3 cm, they are well fit with $B_3 \approx 0.85$. We show that to within experimental error,

this exponent is the same as that reported in the literature for basaltic lavas, and other volcanic products. The importance of the scaling of vesicle distributions is highlighted by the observation that they are particularly effective at “packing” bubbles allowing very high vesicularities to be reached before the critical percolation threshold, a process which—for highly stressed magmas—would trigger explosion. In this way the scaling of the bubble distributions allows them to be key actors in determining the rheological properties and in eruption dynamics.

Keywords Gas vesicles - Scaling - Explosive volcanism - Vesiculation - Fragmentation - Plinian pumices - Coalescence.

Editorial responsibility: D. Dingwell

Introduction

Vesiculation and fragmentation of magmas greatly influence the magnitude of volcanic explosive energies and contribute significantly to total atmospheric gas emissions; their understanding has long challenged geologists (e.g., Sparks *1978*; Papale and Dobran *1993*; Thomas et al. *1994*; Gardner et al. *1996*; Kaminski and Jaupart *1998*; Papale *1999*). At depth magma is mostly dominated by a bubble-free liquid phase; as the magma ascends it reaches a saturated or supersaturated level where bubble nucleation occurs (Mangan and Sisson *2000*). These small bubbles grow at first by diffusion and decompression (e.g. Sparks *1978*) and then, as increasingly recognized, by coalescence (Herd and Pinkerton *1997*; Klug et al. *2002*; Polacci et al. *2003*) and even binary (Lovejoy et al. *2004*) and multibubble coalescence decompressive expansion (Gaonac'h et al. *2003*). Finally the highly vesicular magma undergoes fragmentation (Kaminski and Jaupart *1998*). Although in classical fragmentation processes bubbles play only a passive role, in new percolation models (Gaonac'h et al. *2003*) they play a fundamental active role. At a critical vesicularity, the bubbles join together to form infinite networks catastrophically weakening the magma. In this way bubbles are central at each phase of the eruption and its aftermath.

Many studies have examined the small to medium vesicles present in silicic magmas and interpreted their vesicle size distributions (VSD's) purely in terms of nucleation, diffusion and decompression, hypothesizing them to be from a narrow range of size distributions (often exponential; Cashman and Mangan *1994*; Klug and Cashman *1994*; *1996*). In these frameworks, the largest vesicles are not adequately treated even though they can easily dominate the total vesicularities. In contrast Gaonac'h et al. (*1996b*) showed that in basaltic lavas, power law (scaling) VSD's better represent the overall size distribution of vesicles, with the cumulative number size distribution per unit volume a power law of V where V is the vesicle volume. The 3-dimensional scale invariant exponent, B_3 , has a value of ≈ 0.85 from $500 \mu\text{m}$ to a few cm. An obvious and important characteristic of power laws is that they relate the gas vesicles from one scale or size to another in a way that does not involve a characteristic size. They can be represented by a linear trend in a \log_{10} - \log_{10} diagram between all the measured sizes.

More recently, empirical power law VSD's in explosive (Gaonac'h et al. *1997*; Simakin et al. *1999*; Klug et al. *2002*) volcanic products as well as in laboratory experiments (Simakin et al. *1999*; Blower et al. *2001*) have been found, with B_3 values not far from 0.85 (see below). To explain this behavior, mechanisms that repeat themselves from scale to scale are required; several have been proposed, the basic one being binary coalescence (an effective collision between two bubbles) which under relatively general conditions leads to power law VSD's (Gaonac'h et al. *1996a*, Lovejoy et al. *2004*). Recently, Gaonac'h et al. (*2003*) have suggested that in high vesicularity magmas ternary and higher order multibubble coalescence could give rise to a slightly larger B_3 (the theoretical value is $B_{3,\text{per}}=1.186$) for magma near the critical percolation point. In such a scenario bubbles join into an infinite network possibly causing the fragmentation of the magma. However, empirical values are invariably from 2-D cross-sections; the corresponding values are extrapolated to 3-D by assuming convex bubbles leading to a theoretical value $B_{2-3,\text{per}}=1.037$. The difference between $B_{3,\text{per}}$ and $B_{2-3,\text{per}}$ is due to the nonconvexity of the bubbles. This is very close to the scale invariant exponent of 1.1 ± 0.1 found by Klug et al. (*2002*). Finally, Blower et al. (*2001*) suggested a noncoalescence mechanism based on a nucleation-diffusion process occurring in a fractal hierarchy leading to a $B_3 \sim 0.82$. In addition on purely empirical grounds, Gaonac'h et al. (*1996a*) suggested that the very small bubbles dominated by diffusion-decompression growth also have a power law regime, although with a lower B_3 value of ≈ 0 (Gaonac'h et al. *1996a*).

The scaling of vesicle size distributions is a central notion in theories of bubble growth and magma fragmentation (Gaonac'h et al. 1996a; Lovejoy et al. 2004). In spite of the emerging consensus about power law VSD's, even for a single type of volcanic product, there is no consensus on the unicity of the exponents (e.g. two basic values, one for the binary coalescence, another one for the multibubble coalescence), nor the corresponding range of scales over which the scaling holds. The resolution of these issues has immediate bearing on the debate about the bubble growth mechanisms, and hence on the implications on the possible fragmentation of the magma. In this paper we present additional empirical evidence in favor of power law distributions of vesicle size distributions in Plinian fallout products and propose a unifying explanation for the different observed exponents including those from Plinian and effusive samples. Because the basic value (0.85) allows particularly efficient packing of small bubbles between larger ones, the creation of infinite bubble networks (percolation) is postponed until quite large vesicularities are reached ($\approx 70\%$), thus potentially explaining the eruption as a critical percolation process (Gaonac'h et al. 2003).

Scale invariant distributions

In a scaling regime, the number density $n(V)$ of the vesicles (mm^{-6}) in each sample is a power law as a function of V , the volume of the gas vesicle (Gaonac'h et al. 1996b):

$$n(V) \propto \left(\frac{V}{V^*} \right)^{-B_3-1} \quad (1a)$$

where B_3 is the 3-D scale invariant exponent. When $B_3 < 1$, the scaling must have an upper bound which we will take as V^* . For $B_3 < 1$, The total vesicularity P of the sample is given by:

$$P = P^* \left(\frac{V}{V^*} \right)^{1-B_3} \quad V \leq V^* \quad (1b)$$

It is much easier to study vesicle area distributions from sample cross-sections rather than vesicle volume distributions. In Gaonac'h et al. (1996b) we developed a method for such 2-D analyses. It is convenient to use cumulative number distributions which provide a more regular trend than number densities. We therefore introduced in Gaonac'h et al. (1996b) for 2-D measurements:

$$N_2(A' > A) \approx N_2^* \left(\frac{A}{A^*} \right)^{-B_2} \quad A \ll A^* \quad 0 < B_2 < 1 \quad (2a)$$

$$N_2(A' > A) \approx N_2^* \left(\frac{A}{A^*} \right)^{-B_2} \quad A < A^* \quad B_2 < 0 \quad (2b)$$

where $N_2(A' < A)$ and $N_2(A' > A)$ are the increasing and decreasing cumulative numbers of vesicles per unit area, respectively smaller and larger than A (referred to $N_2(\text{mm}^{-2})$ in the figures). A^* and N_2^* correspond to the characteristic areas and characteristic cumulative number densities of the distributions; the subscript indicates the dimension of space. The notation is borrowed from probability theory where $\Pr(A' > A)$ denotes the probability of a random vesicle A' exceeding a fixed A .

For convex bubbles, the relation between the 2-D and 3-D exponents is particularly simple (Gaonac'h et al., 1996b):

$$B_3 = \frac{2}{3}B_2 + \frac{1}{3} \quad (3)$$

$$N_3^* = \frac{N_2^*}{\sqrt{A^*}} \quad (4)$$

Strictly speaking these results are only valid for convex bubbles such as those commonly found in basalts. However, at high vesicularities, bubbles can be extremely complex and non convex, and a single such bubble when viewed in cross section may appear as several. Thus, equations (3,4) must be used with caution. This is why for the pumice analyzed below we do not attempt to extrapolate our distributions from areas to volumes (see Gaonac'h et al. 2003 for discussion).

Plinian pumice vesicles

There is a growing need to characterize the very large range of vesicle sizes observed in Plinian samples, as well as in other types of volcanic products. Here we present some new analyses and then compare them with published vesicle size distributions. The samples analyzed have been produced by the Plinian Minoan and Middle Pumice eruptions at Santorini volcano (see Gardner et al. 1996 for more details). The Plinian pumices were prepared and analyzed on a cm-scale using the method developed by Gaonac'h et al. (1996b). Some samples were sawn in two perpendicular sections to display the effect of crosscutting, elongated vesicles on the size distribution. The same samples were analyzed using back-scattered electron microscopic images at the micron-scale. Fig. 1 shows examples at various scales. In each case, vesicles of very different sizes are heterogeneously spatially distributed. Their shapes are very irregular and suggest intense coalescence of smaller bubbles. In some samples, vesicles appear elongated in variable directions, presumably due to strain forces (e.g., Fig. 1e). While some authors have proposed that bubbles continue to expand after fragmentation (Gardner et al. 1996), their deformation is more commonly thought to occur during pre-fragmentation processes where shear stresses in the magmatic conduit could be locally very strong (Klug et al. 2002; Polacci et al. 2001,

2003). Moreover, Gardner et al. (1996) suggested that the expansion of the bubbles should be limited when magmas are viscous, as is the case for the Minoan volcanic pumices. We therefore assume that our Plinian samples mostly reflect the pre-fragmentation state of bubble distributions. Finally, we note that deformation of the bubbles does not necessarily modify the scaling behavior of the vesicle size distributions.

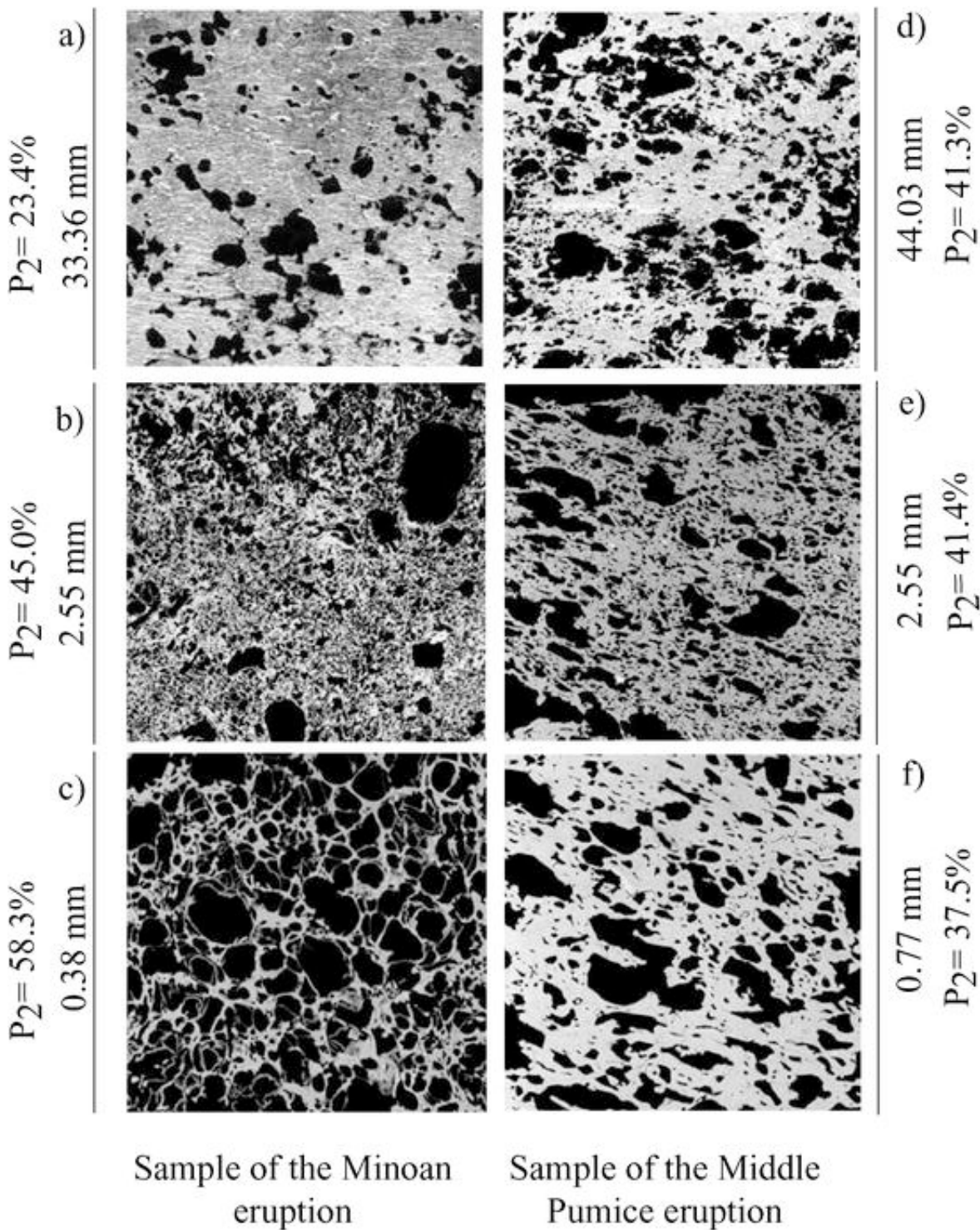


Fig. 1 Digitized sections of a Minoan eruption sample at various resolutions: a, b and c; digitized sections of a Middle Pumice eruption sample at various resolutions: d, e, and f. The viscosities of the degassed magma were 5×10^6 Pas, 4×10^5 Pas and the eruption temperatures were 870°C , 890°C respectively (Gardner et al. 1996)

By first considering the cm-scale Plinian pumice, we observe a common scaling (power law) behavior of their vesicle distributions with a scale invariant exponent $B_2 \approx 0.75$ ($B_3 \approx 0.85$) indicated by a reference line (Fig. 2). The outer limit of the scaling corresponds to the largest cm-scale vesicle present in each sample (see Table 1, A_{\max} values); the inner limit corresponds to the smallest observable vesicles at this cm-scale resolution (0.085 mm corresponding to the digitized image resolution of 300 dpi). The empirical vesicle size distributions (Fig. 2) are biased by two effects. First, the largest cm-scale vesicles, with areas comparable to the image area, are often truncated so that their areas are artificially low. Second, the smallest vesicle number densities are biased due to insufficient resolution with this method. These two effects cause artificial decreases at both ends of the distributions. With these caveats, we consider that power law fits in Fig. 2 are quite reasonable. We may expect the scaling to continue beyond these two external limits since larger bubbles are present in larger samples and smaller bubbles are evident on magnified images.

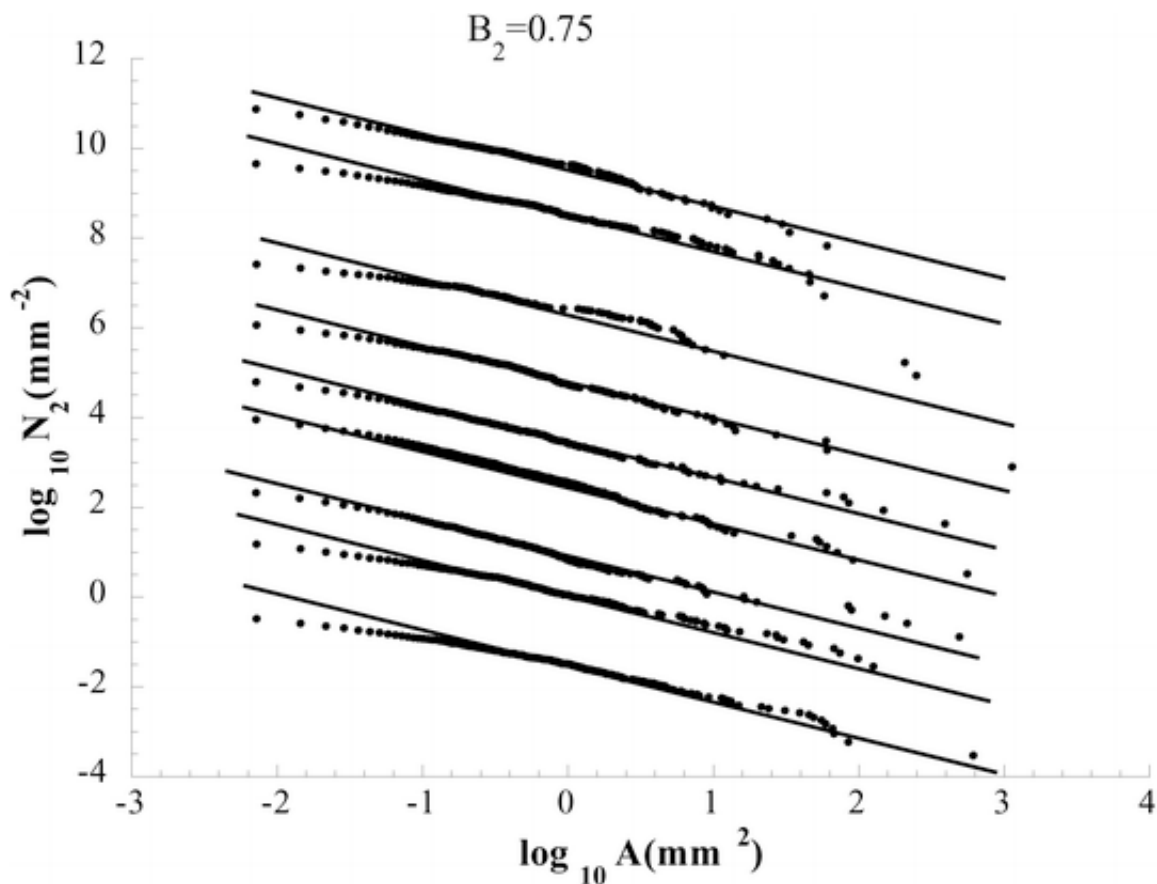


Fig. 2 The cumulative vesicle size distributions $N_2(A^f > A)$ of Middle Pumice and Minoan cm-scale samples show a common scaling behavior described by a reference line with a slope (scale invariant exponent) $B_2 \approx 0.75$ ($B_3 \approx 0.85$). For clarity, starting at the bottom, the n th curve has been offset vertically by $(n-1)$ orders of magnitude. The two top plots are from a single Minoan sample cut along two perpendicular directions (to study possible effects of anisotropy); the others are Middle pumice

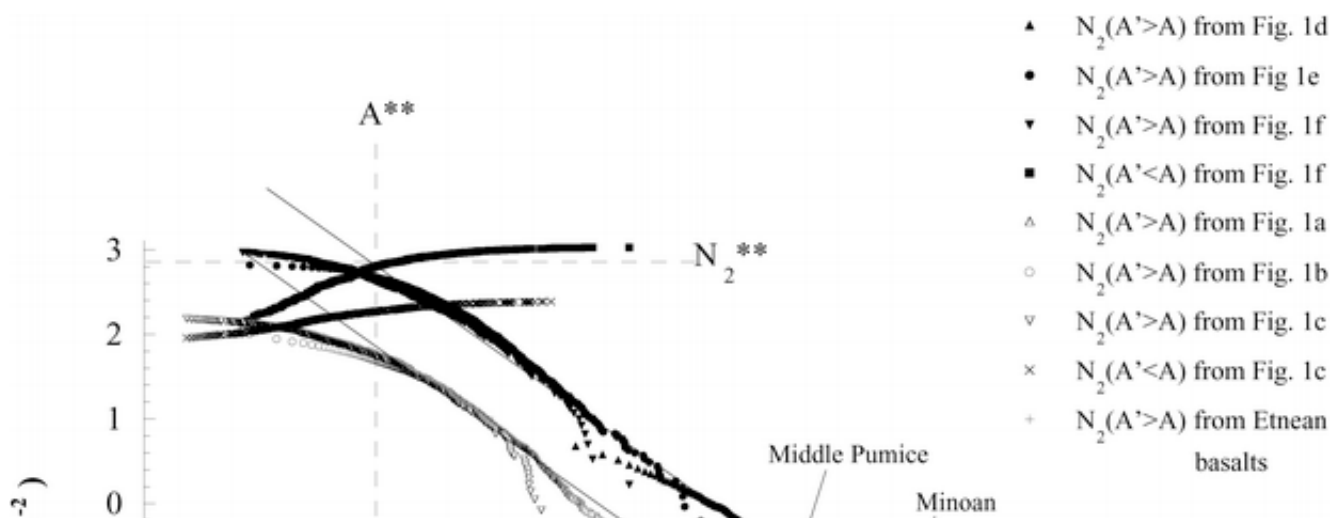
Table 1 Estimates of the largest vesicle size (A_{\max}) are based on the macroscopic sample; the vesicularity (P_{\max}) is based on the largest vesicle (A_{\max}) and the total vesicularity (P_{total}) of the pumice sample

Sample	A_{\max} (mm ²)	P_{\max} (%)	P_{total} (%)
Middle Pumice	611.5	18.3	47.8

Middle Pumice	125.8	5.7	41.3
Middle Pumice	492.7	19.9	55.2
Middle Pumice	558.0	18.5	47.5
Middle Pumice	392.9	16.6	47.8
Middle Pumice	1132.1	39.5	54.4
Middle Pumice	248.0	20.4	49.5
Minoan	57.9	3.3	32.1
Minoan	60.4	4.7	31.6

Eq. 1b shows that for $B_3 < 1$ the variability of the vesicularity P of a pumice largely may be explained by the presence or absence of large vesicles. This theoretical result (Gaonac'h et al. 1996a) is also confirmed in the Santorini pumice samples. The contribution of the vesicularity (P_{\max} in Table 1) of the largest vesicle (for example 1132.1 mm^2 , see Table 1) to the total vesicularity (P in Table 1) in the samples studied varies from 10% ($3.3/32.1$ for a Minoan sample) to 73% ($39.5/54.4$ for a Middle Pumice sample). Such domination by the few largest vesicles to the total vesicularity of a sample has important consequences for estimates of the amount of degassing and for bubble growth dynamics.

For investigation at higher resolutions, we have analyzed Plinian micron scale images. While data from the different scale ranges (e.g., Fig. 1a,b,c for a Minoan sample) are grouped in a single diagram (Fig. 3), we note the same decreases at large and small volumes of each data set as in Fig. 2. In addition, there is another more subtle bias which must be taken into account when comparing enlarged microscopic sections with macroscopic centimeter sized samples. This arises because each micron scale sample (e.g., Fig. 1c, where the size of the image is millimetric) is deliberately selected from a plain region of a larger sample area (e.g., Fig. 1a) situated between millimeter or centimeter sized vesicles; if we had randomly chosen the micro-scale data sets, we would have often selected void vesicle sections of micron or larger dimensions. In other words our microscopic sampling is conditioned on the absence of large vesicles. Such biases lead to micron-scale vesicle cumulative numbers which are artificially too high when considering the whole cm- range of scales (e.g., Fig. 1a). This multiplicative bias, which grows with "zooming", has been removed by translating $\log_{10}N_2 (\text{mm}^{-2})$ downwards by an appropriate amount (by $-0.8, -1.4, -0.7, -1.0$ for Fig. 1b, c, e, f, respectively; see below for discussion). The translation is performed so that the cumulative numbers of medium to large vesicles of the micron scale image of a pumice sample overlap vesicles of similar area from the cm-scale image. Such processing effectively renormalizes the micro-scale count over the whole sample surface.



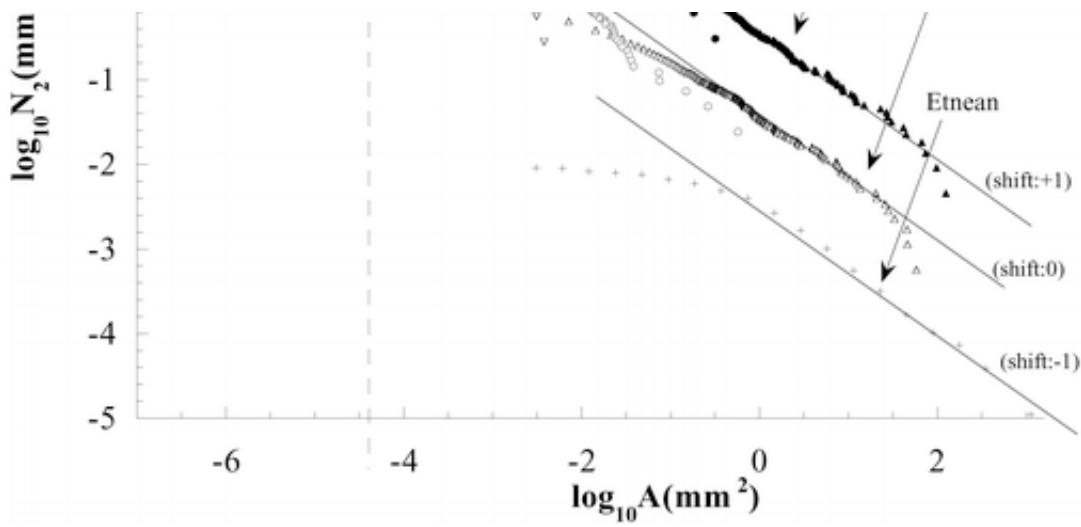


Fig. 3 A comparison of a Middle pumice distribution (top, shifted upwards by a factor of 10 for clarity), a Minoan Pumice (middle) and the mean of over a dozen Etnean basaltic lavas (bottom, shifted downwards by a factor of 10, from Gaonac'h et al. 1996b). The symbols for $N_2(A' > A)$ are: empty triangles (from Fig. 1a), empty circles (from Fig. 1b), empty reversed triangles (from Fig. 1c), filled triangles (from Fig. 1d), filled dots (from Fig. 1e), filled reverse triangles (from Fig. 1f). The symbols for $N_2(A' < A)$ are "x"s (from Fig. 1c) and the filled squares (from Fig. 1f). Crosses are for Etnean $N_2(A' > A)$ distributions. The reference slopes ($\approx -B_2$) are -0.75 for $N_2(A' > A)$ and 0.45 for the Middle Pumice $N_2(A' < A)$ distribution (the best theoretical fit for Minoan is 0.20). The symbols A^{**}_2 and N^{**}_2 , presented for the Middle Pumice sample, represent the upper end of the small vesicle range and the beginning of the medium to large vesicle regime. Note that for the lavas, $B_2 \approx 0.8$ provides a slightly better fit

In Fig. 3 the $B_2 \approx 0.75$ reference line for Middle Pumice and Minoan samples indicates that this power law behavior may extend from the largest observable vesicle down to the characteristic size A^{**} ($10^{-4.3} \text{ mm}^2$ equivalent to $\sqrt{A^{**}} \approx 10 \text{ } \mu\text{m}$ for Middle Pumice) and characteristic number N_2^{**}

($N_2^{**} = 10^{1.8} \text{ mm}^{-2}$ equivalent to $N_3^{**} \approx 10^{13} \text{ m}^{-3}$ for Middle Pumice). As can be seen from the figure in several instances, the lower limits of the $B_2 \approx 0.75$ regime roughly coincide with the upper limits of a small bubble $B_2 < 0$ ($N_2(A' < A)$) regime, hence the double star notation A^{**} and N_2^{**} . Analyses of additional micro-scale samples confirm the same exponent and show $\sqrt{A^{**}}$ to be between $3 \text{ } \mu\text{m}$ and

$10 \text{ } \mu\text{m}$. Etnean lava vesicle distributions shown for comparison confirm that the exponent $B_2 \approx 0.75$ closely fits the distributions for all the products. However, the Plinian pumice has much higher cumulative numbers of much smaller bubbles. For example, the lower bounds on the $B_2 \approx 0.75$ regime, A^{**} , is $3 \times 10^{-11} \text{ m}^2$ in pumice ($\log_{10} A(\text{mm}^2) = -4.5$) compared to $3 \times 10^{-7} \text{ m}^2$ ($\log_{10} A(\text{mm}^2) = -0.5$) in Etnean basalt (Gaonac'h et al. 1996b), corresponding to 100 times smaller linear sizes of pumice bubbles. To compare the pumice and basalt values, the parameter N_2^{**} as presented in Fig. 3 is not so useful since it is estimated at very different A^{**} . If in both cases we consider the number which exceeds the fixed reference value 1 mm^2 , we find $N_2(>1 \text{ mm}^2) \approx 5 \times 10^4 \text{ m}^{-2}$ ($\log_{10} N_2(/ \text{mm}^2) = -1.3$), $3 \times 10^4 \text{ m}^{-2}$ ($\log_{10} N_2(/ \text{mm}^2) = -1.5$) for the mean pumice and mean basalt, respectively, corresponding to a small decrease in the amplitude of the basalt cumulative number.

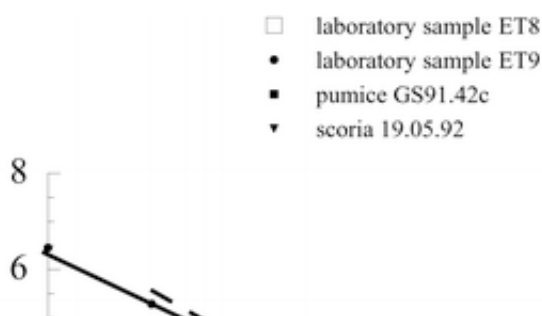
It is also of interest to estimate the total bubble number density of each pumice sample. We first

remark that the combination of macroscopic/microscopic distributions in Fig. 3 has allowed us to eliminate the bias that would be introduced by normal use of SEM imagery. With this adjustment, the total number per unit area larger than the minimum resolution ($0.3 \mu\text{m}$, $1.26 \mu\text{m}$ for Figs. 1c, 1f, respectively) estimated over the observed range is $N_{2,\text{tot}} \approx 10^8 \text{ m}^{-2}$ corresponding to $N_{3,\text{tot}} \approx 3 \times 10^{14} \text{ m}^{-3}$ which is comparable to other published pumice data (Klug and Cashman 1994; Polacci et al. 2001; Klug et al. 2002). However, before using these values as estimates of the absolute total number density, we must verify that we have not missed too many sub-micron bubbles. To do this, we formulate a hypothesis regarding the small bubble distribution. If it also is considered as a power law, Fig. 3 indicates that below A^{**} , the pumice vesicles have $B_2 \approx -0.20$ ($B_3=0.20$) for the Minoan samples and $B_2 \approx -0.45$ ($B_3=0.03$) for the Middle Pumice samples. Unfortunately, exponents $B_3 > 0$ ($N_3 \propto V^{-B_3}$) imply a divergence in N_{tot} due to small bubbles; since this B_3 is so close to the critical value of 0, we conclude that we need higher magnification SEM images in order to obtain correct estimates. The cited values for N_{tot} are simply lower bounds.

Discussion

Simakin et al. (1999), Blower et al. (2001) and Klug et al. (2002) also obtained power law bubble distributions in various samples but the authors claimed a range of exponents. Since a priori, a binary coalescence-decompression mechanism would tend to generate distributions with the same scale invariant exponent, even if many details of the process were different (Gaonac'h et al. 1996a), it is important to test the hypothesis of one or two exponents (one for binary, one for multibubble coalescence) with as many data sets as possible. We therefore reanalyzed the several accessible published power law distributions. The distributions were obtained by extrapolating from 2-D to 3-D using the equivalent of eq. 3 i.e., by implicitly assuming bubble convexity.

Fig. 4 shows natural data from Simakin et al. (1999) with a scale invariant exponent compatible with $B_3 \approx 0.85$ (hence $B_2 \approx 0.75$). However, on the same figure, we also show the distributions of their high vesicularity laboratory samples that displayed coalescence. The low volume regime of these data is reasonably fit by $B_3 \approx 0.85$, but the large volume part is a bit steeper. It may be a reflection of the presence of another exponent. This is possible because Gaonac'h et al. (2003) show that when nearing the percolation threshold (numerically estimated as $70 \pm 5\%$ vesicularity for $B_2=0.75$), the percolation can become dominant with a theoretical value of $B_{2-3,\text{per}} \approx 1.037$, close to the 1.1 ± 0.1 value found in Klug et al. (2002). The $B_3=0.85$ value is only appropriate for binary coalescence. Alternatively, the higher value compared to $B_3=0.85$ may be an artifact resulting from attempts to “decoalesce” bubbles. Since the larger bubbles are likely to be preferentially decoalesced, this could systematically decrease the number of large bubbles with respect to small bubbles and hence raising B_2 and B_3 values.



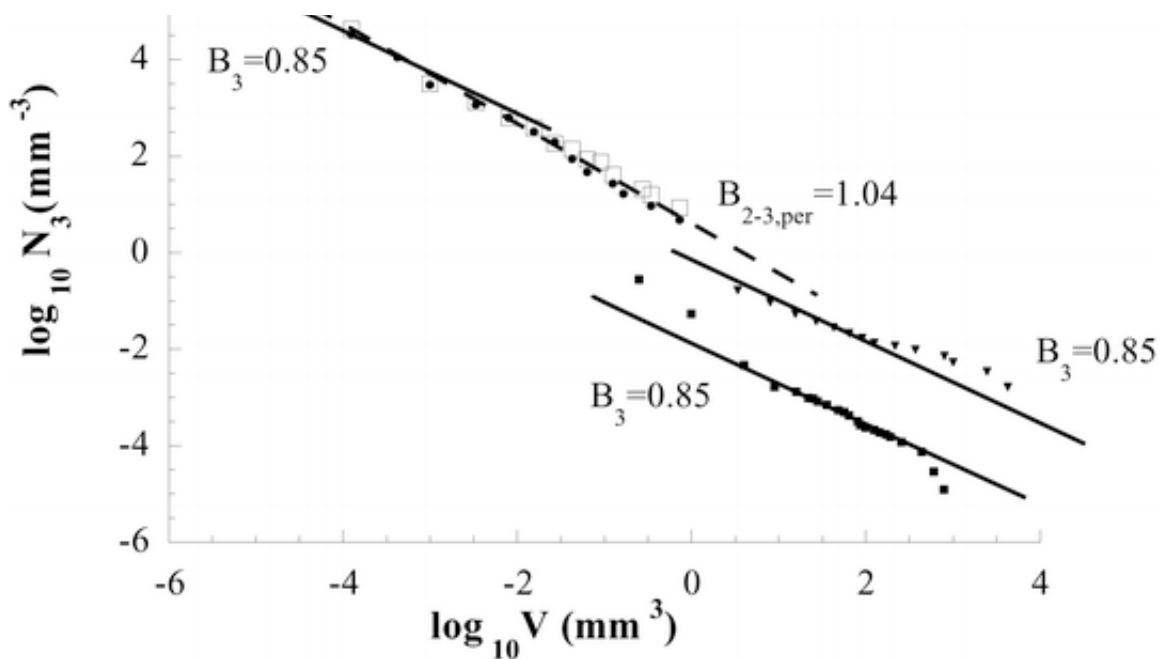


Fig. 4 Replotted from Simakin et al. (1999), this figure demonstrates scaling behavior of pumice (sample GS91.42c, filled squares), scoria (sample 19.05.92, triangles) as well as laboratory samples (those exhibiting coalescence: ET8 squares, ET9, circles). The $B_3 \approx 0.85$ reference line fits most of the data; the $B_3 \approx 1.037$ reference line (the theoretical percolation exponent) gives a slightly better fit to the largest laboratory vesicles

Gaonac'h et al. (2003) show that power law bubble distributions with exponent near the observed value are particularly efficient in “packing” bubbles. This is important since percolation theory shows that otherwise monodisperse distributions with a vesicularity of only 29% would already yield overlapping bubbles, the largest of which would almost surely span an infinite system implying fragmentation at unrealistically low vesicularities. In highly stressed conditions, this would imply explosions at these unrealistically low vesicularities. Gaonac'h et al. (2003) quantitatively show how the observed power law distributions delay such explosive “percolation” until the observed high vesicularities ($\approx 70\%$) are reached.

In this picture, the similarities and differences between effusive and explosive products are relatively straightforward to explain. At small scales, nucleation, diffusion and decompressive expansion create a population of bubbles from sub micron scales up. As the magma violently ascends during a Plinian eruption, acceleration of the magma and rapid expansion of the bubbles induce shear stresses causing locally intense deformation of the bubbles which in turn favour coalescence, especially for the largest bubbles. Observations of Plinian pumice samples confirm the common occurrence of deformed and coalesced vesicles, such as in Fig. 1. The complex anisotropic texture of pumice directly reflects the shear stresses present in the magma (Polacci et al. 2001; Polacci et al. 2003; Klug et al. 2002). Extensive local shearing may eventually lead to the formation of pumice tubes (Polacci et al. 2003; Marti et al. 1999). On a particularly anisotropic sample, we were able to confirm that deformation of bubbles still respects scale invariant properties (Lovejoy et al. 2004).

Because of the generality of the coalescence mechanism and its robustness in yielding power law distributions, this basic model can apply to both explosive and effusive eruptions. In the case of an explosive eruption, the vesicularity is high while great stresses combined with bubble expansion produce shear, bubble overlap and coalescence. At first the vesicularity is low enough so that only two bubble (binary) interactions occur, while at higher vesicularities overlap/coalescence becomes extensive. In multibubble processes, a new exponent characterizes the distributions of the largest

bubbles. Finally, as the critical percolation threshold is approached, coalescence is so extensive that the magma begins to fragment. At the 3D percolation point a single bubble spaghetti-like effectively spans an arbitrarily large section of magma; at the slightly higher 2D percolation point, any planar cross-section is almost certainly cleaved by an infinite bubble. Presumably, the stressed magma will explode somewhat before this point is reached. In effusive eruptions, the initial steps (nucleation, diffusive growth, then binary and multibody coalescence decompressive -expansion) may occur in rather similar ways, although at different rates, and with perhaps different causes of shearing. The key difference is that in effusive eruptions, the existence of an infinite bubble network would have little rheological significance, although it would presumably favour degassing. The basic processes can then continue quite a bit longer than in the explosive stressed case. This would give sufficient time for the nucleation/diffusion processes to exhaust the source of dissolved gas, and the bubbles would have the time to reach near atmospheric pressures. In these circumstances, as long as shearing is still present, coalescence will continue until the liquid bubbly magma reaches the surface. According to the coalescence equation, its effect will be to increase both the lower and upper scaling limits V^{**} and V^* of coalescence while simultaneously decreasing the number densities. By contrast for $B_3 > 1$, pure coalescence would increase the number densities (Lovejoy et al. 2004). This picture thus explains the key similarities and differences of the vesicle size distributions of pumice and basaltic lavas.

Conclusions

Explosive volcanic products commonly display bubbles with sizes ranging from sub micron to centimeters. There is now a growing consensus that to adequately characterize distributions with such huge ranges, power law approaches are required. However, we expect that different exponents correspond to different mechanisms; it is therefore important to systematically analyze samples of as many different products as possible, over as wide a range scale as possible. We have presented systematic studies of macroscopic analyses of 9 Plinian pumice samples including two with joint microscopic analyses. This is the first time that samples have been analyzed over 8 orders of magnitude in bubble areas (12 in volumes) from micron to centimeter scales. A method has been developed in order to avoid overestimating the contribution of small bubbles when comparing microscopic and macroscopic samples; this permitted a more precise estimate of the total number density of Plinian pumice vesicles. We found an overall scaling of over 9 orders magnitude in bubble volumes, and exponents ($B_2 \approx 0.75$, $B_3 \approx 0.85$) which are within statistical uncertainty the same as those found in basalts in Gaonac'h et al. (1996b). We also investigated the prediction, arising from the fact that $B_3 < 1$, that the largest single vesicle could significantly influence the total vesicularity of each sample, leading to large fluctuations in porosity among samples.

Reanalysis of results by Simakin et al. (1999) also supports the scale invariance (power law) characteristic of the vesicle size distributions. The near constancy of the exponent ($B_3 \approx 0.85$) for volcanic products from a wide range of volcanic conditions was predicted in Gaonac'h et al. (1996a) via a cascade-like scaling mechanism. Higher values need to be considered when the pumices exhibit multicoalescence. On the other hand, such samples are more difficult to observe before the percolation and fragmentation of the magma.

While power law distributions have important implications for modeling ascending magmas, perhaps the most important consequences of such distributions are for the fragmentation stage of an eruption. All the contending theories involve highly stressed magmas evolving past critical thresholds. In the classical theories the thresholds are either critical stresses or critical strains. For example, some authors favor brittle fragmentation through a glass transition phase when the magma is under a large strain rate

(e.g., Marti et al. 1999; Papale 1999) or large stresses within bubbles (Zhang 1999). Other authors propose that a downward decompressive wave impinges upon brittle or ductile magma which then exceeds a critical stress for fragmentation (Alidibirov and Dingwell 1996). In these classical models the bubbles play essentially passive roles; they merely prepare the magma rheology which evolves in a continuous way as the vesicularity increases and an external dynamical trigger is necessary for an eruption. We have presented an alternative scenario (Gaonac'h et al. 2003) in which the bubbles play an active role in the sense that the rheology evolves discontinuously with vesicularity; at a critical value of vesicularity, quite independently of the stresses or strains, the magma fragments. This critical vesicularity corresponds to the percolation threshold where bubble overlap is so extensive that an infinite bubble is essentially produced. Under high stress forces, the whole vesiculated system breaks down, and an explosion occurs.

Work in progress involves the analyses and interpretations of vesicle size distributions of explosive products which have evolved in different volcanic conditions. The search for the nature of scaling of bubble distributions represents an important opportunity to better understand the eruptive dynamics of volcanoes.

Acknowledgments We would like to thank C. Jaupart and S. Vergnolle for fruitful discussions as well as support during part of this research. The research has been funded by the Natural Sciences and Engineering Research Council of Canada. This work has been made possible by the hard work of C. Miville who sadly did not live to see the end of the project. We also thank J. Gardner and S. Sparks for constructive criticism of an earlier version, as well as C. Soriano and M. Polacci for constructive criticism of the present version.

References

Alidibirov M., Dingwell D.B. (1996) Magma fragmentation by rapid decompression. *Nature*: 146–148

Blower J.D., Keating J.P., Mader H.M., Phillips J.C. (2001) Inferring volcanic degassing processes from vesicle size distributions. *Geophys Res Lett* 28:347–350



Cashman K.V., Mangan M.T. (1994) Physical aspects of magmatic degassing II. Constraints on vesiculation processes from textural studies of eruptive products. In: Carroll, M.R. and Holloway, J.R. (ed) *Volatiles in magmas*. *Rev. Mineral.* 30, pp 447–478

Gaonac'h H., Lovejoy S., Stix J., Schertzer D. (1996a) A scaling growth model for bubbles in basaltic lava flows. *Earth Planet Sci Lett* 139:395–409



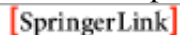
Gaonac'h H., Stix J., Lovejoy S. (1996b) Scaling effects on vesicle shape, size and heterogeneity of lavas from Mount Etna. *J Volcanol Geotherm Res* 74:131–153



Gaonac'h H., Lovejoy S. (1997) Scaling models and analyses of lava and pumice vesicle size distributions abstract, IAVCEI, Mexico

Gaonac'h H., Lovejoy S., Schertzer D. (2003) Percolating magmas and explosive volcanism. *Geophys Res Lett* v 30, no 11, 1159, doi.1029/GL016022, 2003

Gardner J.E., Thomas R.M.E., Jaupart C., Tait S. (1996) Fragmentation of magma during Plinian volcanic eruptions. *Bull Volcanol* 58:144–162

 [SpringerLink]

Herd, R.A., Pinkerton H. (1997) Bubble coalescence in basaltic lava: its impact on the evolution of bubble populations. *J Volcanol Geotherm Res* 75:137–157

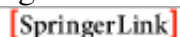
Kaminski E., Jaupart C. (1998), The size distribution of pyroclasts and the fragmentation sequence in explosive volcanic eruptions. *J Geophys Res* 103:29759–779



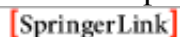
Klug C., Cashman K.V. (1994) Vesiculation of May 18, 1980, Mount St. Helens magma. *Geology* 22:468–472



Klug C., Cashman K.V. (1996) Permeability development in vesiculating magmas: implications for fragmentation. *Bull Volcanol* 58:87–100



 [SpringerLink]

Klug C., Cashman K.V., Bacon C.R. (2002) Structure and physical characteristics of pumice from the climatic eruption of Mount Mazama (Crater Lake), Oregon. *Bull Volcanol* 64:486–501



 [SpringerLink]

Lovejoy S., Gaonac'h H., Schertzer D. (2004), Bubble distributions, and dynamics: the expansion-coalescence equation, submitted to *J Geophys Res* 103, in press



Mangan M., Sisson T. (2000) Delayed, disequilibrium degassing in rhyolite magma: decompression experiments and implications for explosive volcanism. *Earth Planet Sci Lett* 183:441–455


Marti J., Soriano C., Dingwell D.B. (1999) Tube pumices as strain markers of the ductile-brittle transition during magma fragmentation. *Nature* 402:650–653

Papale P., Dobran F. (1993) Modelling of the ascent of magma during the plinian eruption of Vesuvius in A.D. 79. *J Volcanol Geotherm Res* 58:101–132

Papale P. (1999) Strain-induced magma fragmentation in explosive eruptions. *Nature* 397:425–428

Polacci M., Papale P., Rosi M. (2001) Textural heterogeneties in pumices from the climactic eruption of Mount Pinatubo, 15 June 1991, and implications for magma ascent dynamics. Bull Volcanol 63:83–97

[\[SpringerLink\]](#)

Polacci M., Pioli L. and Rosi M. (2003) The Plinian phase of the Campanian Ignimbrite eruption (Phlegrean Fields, Italy): evidence from density measurements and textural characterization of pumice. Bull Volcanol 65:418–432

[\[SpringerLink\]](#)

Sparks R.S.J. (1978) The dynamics of bubble formation and growth in magmas. J Volcanol Geotherm Res 3:1-37

[crossref](#) [ChemPort](#)

Simakin A.G., Armienti P., Epelbaum M.B. (1999) Coupled degassing and crystallization: experimental study at continous pressure drop, with application to volcanic bombs. Bull Volcanol 61:275–287

[\[SpringerLink\]](#)

Thomas N., Jaupart C., Vergnolle S. (1994) On the vesicularity of pumice. J Geophys Res 99:15 633–15 644

Zhang Y. (1999) A criterion for the fragmentation of bubbly magma based on brittle failure theory. Nature 402:648–650

[crossref](#) [ChemPort](#)